Hindawi Publishing Corporation
Mathematical Problems in Engineering
Volume 2007, Article ID 78507, 19 pages
doi:10.1155/2007/78507

Research Article

A Finite Circular Arch Element Based on Trigonometric Shape Functions

H. Saffari and R. Tabatabaei

Received 27 August 2006; Accepted 26 February 2007

Recommended by Jan Awrejcewicz

The curved-beam finite element formulation by trigonometric function for curvature is presented. Instead of displacement function, trigonometric function is introduced for curvature to avoid the shear and membrane locking phenomena. Element formulation is carried out in polar coordinates. The element with three nodal parameters is chosen on curvature. Then, curvature field in the element is interpolated as the conventional trigonometric functions. Shape functions are obtained as usual by matrix operations. To consider the boundary conditions, a transformation matrix between nodal curvature and nodal displacement vectors is introduced. The equilibrium equation is written by minimizing the total potential energy in terms of the displacement components. In such equilibrium equation, the locking phenomenon is eliminated. The interesting point in this method is that for most problems, it is sufficient to use only one element to obtain the solution. Four examples are presented in order to verify the element formulation and to show the accuracy and efficiency of the method. The results are compared with those of other concepts.

1. Introduction

Curved beams are more efficient in transfer of loads than straight beams because the transfer is affected by bending, shear, and membrane action. Some of the structures such as arches and arch bridges are modeled using curved beam elements. The finite element analysis of curved beam has been given significant attention by researchers in recent years mostly because it is a versatile method for solving structural and other mechanical problems.

The analysis of curved beam is conventionally formulated based on displacement fields. Such formulation often leads to excessively stiff behavior in the thin regimes. In such analyses, shear locking phenomenon occurs when lower-order elements are used in modeling. This is because in such models, only flexural deformations are considered and shear deformations are neglected. Another phenomenon is called membrane locking. It occurs when other classical curved finite elements are used for modeling thin and thick curved beams; because they exhibit excessive bending stiffness alone in approximating the extensional bending response and the lower-order element cannot bend without being stretched. It means that elements are unable to represent the condition of zero radial shear strains. Therefore, these two phenomena are associated with highly undesirable situation and numerical deficiency. Thus much attention has been focused to remedy the locking phenomena.

Most of researches have proposed various schemes to alleviate locking such as reduced integration, (Zienkiewicz et al. [1]; Stolarski and Belytschko [2, 3]; Pugh et al. [4]), discrete Kirchhoff's theory (Batoz et al. [5]), penalty relaxation method, (Tessler and Spiridigliozzi [6]), hybrid/mixed concept (Reddy and Volpi [7]), isoparametric interpolations, (Ashwell et al. [8]), free formulation, (Dawe [9]; Ashwell and Sabir [10]), and assumed displacement field (Raveendranath et al. [11]). However, most of these approaches have been used for thin regimes, however the given results have shown that these methods cannot represent the behavior of the curved beam quite correctly in the thick regimes. To overcome this problem, a three-nodded curved beam element is formulated by Bathe [12], considering shear and tangential rigidity. Curved beam element with straight beam elements is modeled Mc Neal and Harder [13]; however this results in a large degree of freedom in a modeling. A three-nodded locking-free curved beam elements based on curvature is formulated by Lee and Sin [14]. The latest attempt by Sinaie et al. [15] considers eliminating shear-locking phenomenon and involves six nodal curvatures. A new two-nodded shear flexibility curved beam element by assuming polynomial radial displacement field is derived by Raveendranath [11]. Shear force effects on curved beam element behavior were considered by Sheikh [16]. Nonlinear formulation of curved beam element by using curvilinear system and neglecting shear force effects is investigated by Wen and Suhendro [17] and Wen and Lange [18] and Calhoun and DaDeppo [19].

In this paper, a new curved beam finite element formulation by trigonometric function for curvature is presented. Unlike other investigators, trigonometric function is used for curvature and this enables efficient elimination of the shear and membrane-locking phenomenon. This is achieved by introducing strain-displacement relationships in polar coordinate system using a three-nodded element. Relationship between nodal curvature and nodal displacement is obtained using transformation matrix. The total potential energy equation is written and minimized; then, force-displacement relation is derived and an algorithm for analysis is proposed. Finally, four numerical examples are solved and the results are compared with solutions given by other methods. The results show that performance of the new-presented element without locking phenomena is preferred over the other types of elements.

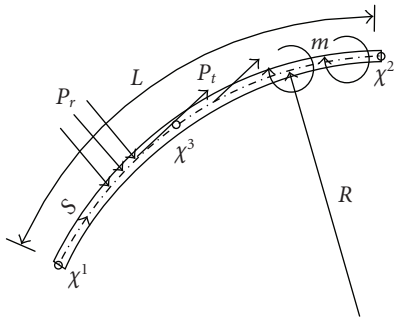

Figure 2.1. Nodal curvatures and applied loads in a 3-node circular arch element.

2. The curvature field and matrix operations

The matrix operation for the curvature χ of circular arch element is being presented in this section (see Figure 2.1). Prior to present the formulation, it is worthy to note here before the formulation that curvature can be interpolated with conventional trigonometric functions. In present study, a three-node element for the curvature is chosen. The shape function for this type of element is the simplest one, which express the behavior of a curved beam. A trigonometric function representation for curvature field χ is assumed as

$$\chi = a_1 + a_2 \operatorname{Cos}(\Phi) + a_3 \operatorname{Sin}(\Phi) \tag{2.1}$$

or

$$\chi = [f] \cdot [a], \tag{2.2}$$

where $[a]$ and $[f]$ are two vectors defined by

$$\begin{aligned} [a]^T &= \begin{bmatrix} a_1 & a_2 & a_3 \end{bmatrix}, \\ [f] &= \begin{bmatrix} 1 & \operatorname{Cos}(\Phi) & \operatorname{Sin}(\Phi) \end{bmatrix} \end{aligned} \tag{2.3}$$

in which Φ is obtained by

$$\Phi = \frac{S}{R}. \tag{2.4}$$

The relation nodal for curvature vector $[\kappa]$ can be written as

$$[\kappa] = [\omega] \cdot [a], \tag{2.5}$$

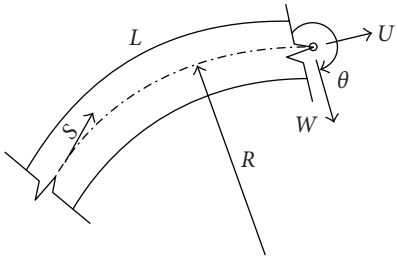

Figure 3.1. Components of displacement in a typical circular arch beam.

where

$$[\kappa]^T = \begin{bmatrix} \chi_1 & \chi_2 & \chi_3 \end{bmatrix},$$
$$[\omega] = \begin{bmatrix} 1 & 1 & 0 \\ 1 & \operatorname{Cos}\dfrac{L}{R} & \operatorname{Sin}\dfrac{L}{R} \\ 1 & \operatorname{Cos}\dfrac{L}{2R} & \operatorname{Sin}\dfrac{L}{2R} \end{bmatrix}. \tag{2.6}$$

Substituting (2.5) in (2.2) results in

$$\chi = [f] \cdot [\omega]^{-1} \cdot [\kappa] \tag{2.7}$$

as depicted in Figure 2.1. If the curvature in the element is interpolated the following equations are obtained:

$$[f_\kappa] = [f] \cdot [\omega]^{-1}, \tag{2.8}$$
$$\chi = [f_\kappa] \cdot [\kappa], \tag{2.9}$$
$$[f_\kappa] = \begin{bmatrix} f_1^\kappa & f_2^\kappa & f_3^\kappa \end{bmatrix}, \tag{2.10}$$
$$f_1^\kappa = \left\{ \frac{1}{4} \left(\operatorname{Cos}\left(\frac{L}{4R}\right) - \operatorname{Cos}\left(\frac{3L-4S}{4R}\right) \Big/ \left(\operatorname{Sin}\left(\frac{L}{4R}\right)^2 \operatorname{Cos}\left(\frac{L}{4R}\right) \right) \right) \right\}, \tag{2.11}$$
$$f_2^\kappa = \left\{ -\frac{1}{2} \left(\operatorname{Sin}\left(\frac{L-2S}{4R}\right) \operatorname{Sin}\left(\frac{S}{2R}\right) \Big/ \left(\operatorname{Sin}\left(\frac{L}{4R}\right)^2 \operatorname{Cos}\left(\frac{L}{4R}\right) \right) \right) \right\}, \tag{2.12}$$
$$f_3^\kappa = \left(\operatorname{Sin}\left(\frac{L-S}{2R}\right) \operatorname{Sin}\left(\frac{S}{2R}\right) \Big/ \operatorname{Sin}\left(\frac{L}{4R}\right)^2 \right). \tag{2.13}$$

3. The sectional rotation field

The geometry of a circular arch element with radius R and centroidal arc length L loaded in plane is shown in Figure 3.1.

Considering the figure, the sectional rotation field θ for a typical circular arch element in polar coordinates is derived using the curvature χ as

$$\chi = \theta_{,S}, \tag{3.1}$$

where subscript S denotes differentiation with respect to arc length. Substituting (2.9) in (3.1) and integrating from (3.1) results in

$$\begin{aligned} \theta &= [f_\theta] \cdot [\kappa], \\ [f_\theta] &= \int_0^S [f_\kappa] \cdot ds + C_1, \end{aligned} \tag{3.2}$$

where C_1 is the integration constant and $[f_\theta]$ is determined as detailed in Appendix A.

4. The radial and tangential displacement fields

The radial displacement W and the tangential displacement U for a typical circular arch element are illustrated in Figure 3.1. The relationships between these components of displacement and the shearing strain γ as well as the tangential strain ε are as follows:

$$\begin{aligned} \varepsilon &= U_{,S} - \frac{W}{R}, \\ \gamma &= W_{,S} - \theta + \frac{U}{R}. \end{aligned} \tag{4.1}$$

The membrane force N, the bending moment M_b, and the shear force V, respectively are given by

$$N = EA\varepsilon, \qquad M_b = EI\chi, \qquad V = kGA\gamma, \tag{4.2}$$

where A is the cross sectional area, I is the moment of inertia, E is the modulus of elasticity, G is shear modulus and k is the shear coefficient. The equilibrium equations of a circular arch element, take the following form (Timoshenko and Gere [20]):

$$\begin{aligned} M_{b,S} + V &= 0, \\ V_{,S} + \frac{N}{R} &= 0, \\ N_{,S} + \frac{M_{b,S}}{R} &= 0. \end{aligned} \tag{4.3}$$

Substituting (4.1) in (4.2) and then in (4.3) yields

$$\begin{aligned} W_{,SS} + \frac{W}{R^2} &= \chi - \left(\frac{EI}{GAk} + \frac{I}{A}\right) \cdot \chi_{,SS}, \\ U &= R \cdot \left(\theta - W_{,s} - \frac{EI}{GAk} \cdot \chi_{,s}\right). \end{aligned} \tag{4.4}$$

Solving (4.4) for the radial and tangential displacements can be calculated in terms of curvature as

$$\begin{aligned} W &= f_W \cdot \kappa + C_2 \cdot \cos(\Phi) + C_3 \cdot \sin(\Phi), \\ U &= f_U \cdot \kappa + R \cdot C_1 + C_2 \cdot \sin(\Phi) - C_3 \cdot \cos(\Phi), \end{aligned} \tag{4.5}$$

where constants, C_1, C_2, and C_3, are the components of rigid-body displacements while f_θ, f_W, and f_U are detailed in Appendix A.

5. Nodal curvatures and nodal displacements relation

Consider a circular arch element with six specified boundary conditions as shown in Figure 3.1. By applying boundary conditions to nodes 1 and 2, the deformation-curvature relations are obtained as

$$W_1 = f_W\big|_{S=0} \cdot \kappa + C_2, \tag{5.1}$$

$$U_1 = f_U\big|_{S=0} \cdot \kappa + R \cdot C_1 - C_3, \tag{5.2}$$

$$\theta_1 = f_\theta\big|_{S=0} \cdot \kappa + C_1 = C_1, \tag{5.3}$$

$$W_2 = f_W\big|_{S=L} \cdot \kappa + C_2 \cdot \cos\frac{L}{R} + C_3 \cdot \sin\frac{L}{R}, \tag{5.4}$$

$$U_2 = f_U\big|_{S=L} \cdot \kappa + R \cdot C_1 + C_2 \cdot \sin\frac{L}{R} - C_3 \cdot \cos\frac{L}{R}, \tag{5.5}$$

$$\theta_2 = f_\theta\big|_{S=L} \cdot \kappa + C_1, \tag{5.6}$$

where $f_i|_{S=a}$ is the value of f_i at $S = a$. Substituting (5.1)–(5.3) in (5.4)–(5.6), respectively, and eliminating the constants C_1, C_2, and C_3, the nodal displacements and nodal curvature obtained as

$$[T_\kappa] \cdot [\kappa] = [T_u] \cdot [\delta], \tag{5.7}$$

where $[\delta]$ is the boundary condition vector and is defined as

$$[\delta] = \begin{bmatrix} U_1 & W_1 & \theta_1 & U_2 & W_2 & \theta_2 \end{bmatrix}^T,$$

$$[T_\kappa] = \begin{bmatrix} f_W\big|_{S=L}\kappa - f_W\big|_{S=L}\cos\dfrac{L}{R} + f_U\big|_{S=0}\sin\dfrac{L}{R} \\ f_U\big|_{S=L}\kappa - F_W\big|_{S=0}\sin\dfrac{L}{R} - f_U\big|_{S=0}\cos\dfrac{L}{R} \\ f_\theta\big|_{S=L} \end{bmatrix},$$

$$[T_u] = \begin{bmatrix} -\cos\dfrac{L}{R} & \sin\dfrac{L}{R} & -R\sin\dfrac{L}{R} & 1 & 0 & 0 \\ -\sin\dfrac{L}{R} & -\cos\dfrac{L}{R} & -R\left(1-\cos\dfrac{L}{R}\right) & 0 & 1 & 0 \\ 0 & 0 & -1 & 0 & 0 & 1 \end{bmatrix}. \tag{5.8}$$

The transformation matrix $[T]$, which relates the nodal curvature vector and the nodal displacement vector, may be expressed as follow:

$$[T] = \left[T_{\kappa}^{-1}\right] \cdot [T_U], \qquad [\kappa] = [T] \cdot [\delta]. \tag{5.9}$$

6. Equilibrium equation of the element

The finial finite element equilibrium equation is written in terms of the displacement components of the two nodes. The shear and tangential strains are incorporated into the total potential energy by the force equilibrium equation. Therefore, the presented analysis formulation of the circular arch element is ensured to be free of the locking phenomena. The total potential energy in a circular arch element shown in Figure 2.1 is written as

$$\pi = \frac{1}{2}EI\int_0^L \chi^2\,ds + \frac{1}{2}GAk\int_0^L \gamma^2\,ds + \frac{1}{2}EA\int_0^L \varepsilon^2\,ds - [P_e]. \tag{6.1}$$

In the above equation, P_e is the equivalent nodal load vector. Considering the expression for each strain and displacement field and invoking the stationary condition of the given system, that is, $\delta\pi = 0$ the relation between force and displacement is obtained in the following steps:

$$[K] \cdot [\delta] = [P_e]. \tag{6.2}$$

The stiffness matrix $[K]$ is given by

$$[K] = [T]^T \cdot \left[EI\left(\int_0^L f_{\kappa}^T \cdot f_{\kappa}\,dS + \alpha\int_0^L f_{\kappa,s}^T \cdot f_{\kappa,s}\,dS + \beta\int_0^L f_{\kappa,ss}^T \cdot f_{\kappa,ss}\,dS\right)\right] \cdot [T] \tag{6.3}$$

and the equivalent nodal load vector $[P_e]$ is obtained by:

$$[P_e] = \int_0^L V_W^T \cdot P_r \cdot dS + \int_0^L V_U^T \cdot P_t \cdot dS + \int_0^L V_{\theta}^T \cdot m \cdot dS, \tag{6.4}$$

where P_r, P_t and m are the distributed radial, tangential, and moment loads applied, respectively, as shown Figure 2.1. The V_W, V_U and V_θ are defined later in Appendix B.

7. Numerical studies

Four sample problems of a curved beam are solved in this section. (1) An arc for various subtended angles supported on a fixed and a roller at the other end. (2) A quarter circular cantilever circular arch. (3) A pinched ring and (4) A quarter circular arch with a moment load applied. These problems are elaborately selected because they are of typical theoretical studies to investigate shear and membrane-locking phenomena. Comparison of the results obtained in this study is shown with those obtained by other investigators.

7.1. Example 1: an arc for various subtended angles. An arc of a ring with angle α and with one end fixed and a concentrated load P at the other roller end, as in Figure 7.1, is characterized by slenderness, $R/h = 50$. The vertical displacements obtained under load

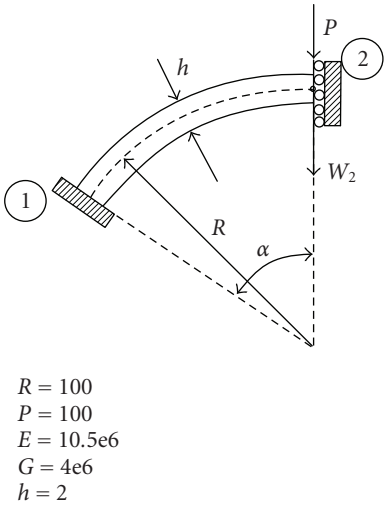

Figure 7.1. An arc for various subtended angles α.

Table 7.1. Comparison of the finite element solution (radial displacement under load) of one-quarter ring with other methods.

Angle α (degree)	Results by Lee and Sin [14]	Results by Raveendranath et al. [11]	Results by Sinaie et al. [15]	One-element present study
10	0.004 19	0.004 19	0.004 19	0.004 19
20	0.007 7	0.007 7	0.007 7	0.007 7
30	0.014 2	0.014 1	0.014 2	0.014 23
40	0.028 7	0.028 6	0.028 7	0.028 76
50	0.054	0.054	0.054	0.054 00
60	0.093 1	0.093 0	0.093 1	0.093 16
70	0.149 9	0.148 5	0.149 9	0.149 95
80	0.228 8	0.227 5	0.228 8	0.228 8
90	0.335 0	0.334 5	0.335 0	0.335 1
100	0.475 0	0.474 5	0.475 0	0.475 2
120	0.889 2	0.889 2	0.889 2	0.889 8
140	1.557 0	1.556 5	1.557 0	1.558 9
160	2.608 9	2.607 8	2.608 9	2.613 8
180	4.240 3	4.240 0	4.240 3	4.253 9

P are compared with those given by the other methods (Raveendranath et al. [11]; Lee and Sin [14] and Sinaie et al. [15]), and are summarized in Table 7.1.

It can be seen, from Table 7.1 that the results of the present analysis agree well with those obtained by other methods. Also, just one element can be calculating accuracy

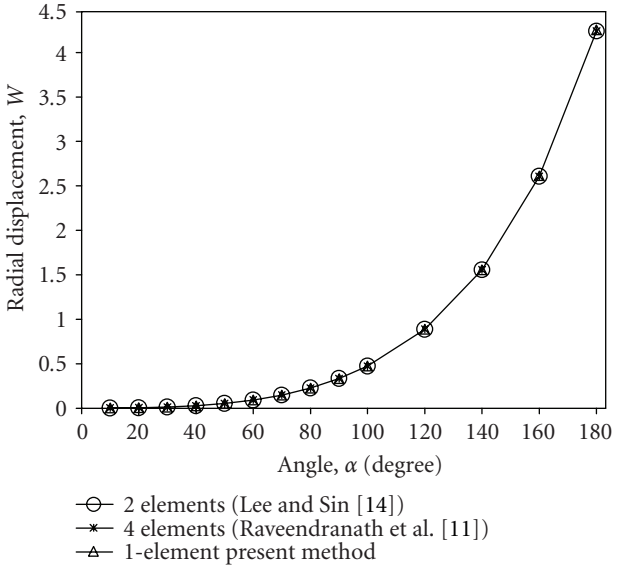

Figure 7.2. Radial displacement under load for various subtended angle α.

results by presented method. Figure 7.2 is the graphical representation of the results by various concepts mentioned above. While the results of present study are superposed. In this figure, the radial displacement of joint 2 of thin arch for various subtended angle α is shown. It can be seen from Figure 7.2 that the solutions given by Raveendranath et al. [11] and Lee and Sin [14] in good agreement with the results obtained by new formulation presented here. It should be remembered that in present study only one element has been employed whereas in other methods, the number of elements are large.

7.2. Example 2: a quarter circular cantilever ring. The details of a quarter circular cantilever ring are shown in Figure 7.3. The finite element results for radial displacement (W), tangential displacement (U), and sectional rotation (θ) at the ring tip and for a wide rang of slenderness, ($R/h = 4$ to 1000, thick to thin) and those obtained by other methods are all summarized in Table 7.2. The free-locking exact solution can be derived analytically using Castigliano's theorem (considering all bending, shear and membrane are strain energy components) and is shown as follows: (Lee and Sin [14])

$$W_c = \frac{\pi PR^3}{4EI} + \frac{\pi PR}{4GAk} + \frac{\pi PR}{4EA}, \tag{7.1a}$$

$$U_c = \frac{PR^3}{2EI} - \frac{PR}{2GAk} - \frac{PR}{2EA}, \tag{7.1b}$$

$$\theta_c = \frac{PR^2}{EI}. \tag{7.1c}$$

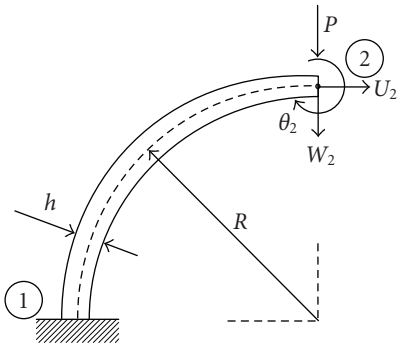

$R = 10$
Unit width
$E = 10.5e6$
$G = 4e6$
$P = 1$

Figure 7.3. A quarter circular cantilever circular arch.

Table 7.2. Comparison of the finite element solution ratio of a quarter circular cantilever circular arch.

Slenderness ratio R/h	Two-element model by Raveendranath et al. [11]			One-element present study		
	$\frac{W_f}{W_c}$	$\frac{\theta_f}{\theta_c}$	$\frac{U_f}{U_c}$	$\frac{W_f}{W_c}$	$\frac{\theta_f}{\theta_c}$	$\frac{U_f}{U_c}$
4	0.997 61	0.999 32	1.034 06	1.000 0	1.000 0	1.033 50
10	0.998 28	0.999 32	1.000 53	1.000 0	1.000 0	1.005 27
20	0.998 37	0.999 32	1.001 28	1.000 0	1.000 0	1.001 31
50	0.998 40	0.999 32	1.000 17	1.000 0	1.000 0	1.000 21
100	0.998 40	0.999 32	1.000 01	1.000 0	1.000 0	1.000 05
200	0.998 40	0.999 32	0.999 96	1.000 0	1.000 0	1.000 01
500	0.998 40	0.999 32	0.999 95	1.000 0	1.000 0	1.000 0
1000	0.998 40	0.999 32	0.999 95	1.000 0	1.000 0	1.000 0

Subscripts f and c denote the finite element solution and analytic solution by Castigliano's theorem, respectively.

Table 7.2 shows the accuracy of the present model and indicates that the results are better than those obtained by other methods.

It is concluded, from the results given in preceding sections, that trigonometric function for curvature concept provides sufficient accuracy while using the least number of elements employed. Moreover, the shear and membrane-locking phenomenon is completely eliminated in this regime.

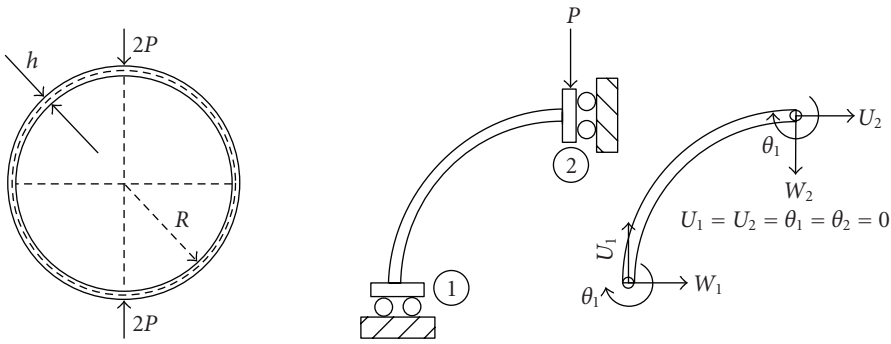

$R = 4.953$
$h = 0.094$
Unit width
$E = 10.5e6$
$G = 4e6$
$P = 100$

(a) A pinched ring

$R = 4.953$
$h = 0.094$
Unit width
$E = 10.5e6$
$G = 4e6$
$P = 100$

(b) 1/4 circular arch with nodal displacement

Figure 7.4. A pinched ring with a load $2P$ and model for 1/4 circular arch.

7.3. Example 3: a pinched ring. Another example, which is studied here, is a pinched ring typically shown in Figure 7.4. The same radial loads are applied at top and bottom of such ring. The ring is modeled by a 1/4 section with the boundary conditions as shown in Figures 7.4(a), 7.4(b) and then analyzed using only one element.

Using Castigliano's theorem, the radial displacement under point load can be obtained as (Lee and Sin [14])

$$W_1 = -\left[\frac{PR^3}{EI}\frac{4-\pi}{2\pi} + \frac{PR}{2GAk} - \frac{PR}{2EA}\right], \tag{7.2a}$$

$$W_2 = \frac{PR^3}{EI}\frac{\pi^2-8}{4\pi} + \frac{\pi PR}{4GAk} + \frac{\pi PR}{4EA}. \tag{7.2b}$$

Figure 7.5 shows the comparison of the finite element results with those of the theoretical solution. In order to better represent the comparison, nondimensional axis is chosen. The ratios of the radial deflection obtained by all methods studied to the results of Castigliano's theorem are shown on abscise. It is mentioned here that again only one element has been employed in present finite element analysis.

The present model yields better result $W_f/W_c = 1.0$ as shown in Figure 7.5. However, results of element by (Raveendranath et al. [11]) are found to yield $W_f/W_c = 0.955$ and formulation of (Sinaie et al. [15]) is reported to yield result, $W_f/W_c = 0.999$. However, the results the other methods for the single element model are not reported here.

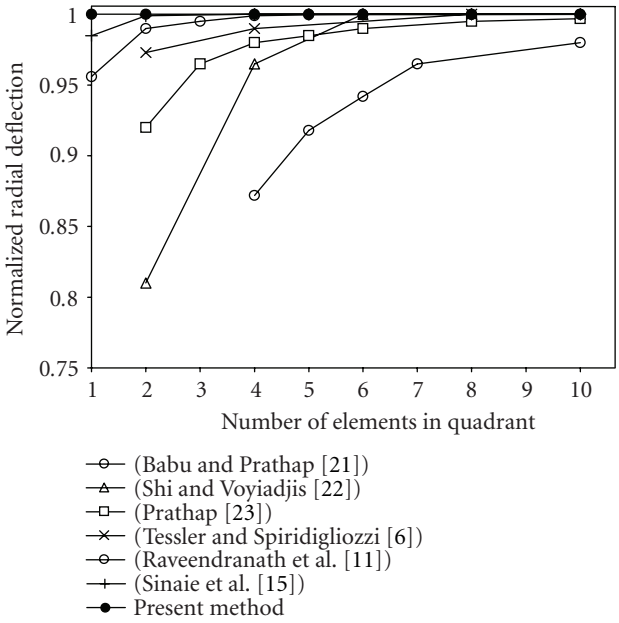

Figure 7.5. Convergence of normalized radial displacement under load $2P$ and model for 1/4.

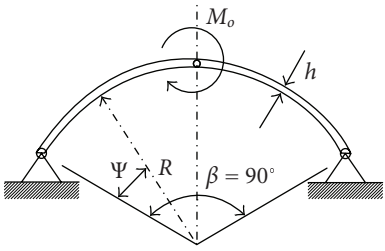

$R = 10$
$h = 0.001$
Unit width
$E = 1.2e10$
$G = 4.615e9$
$M_o = 1$
$\beta = 90^\circ$

Figure 7.6. A half-circular arch with hinged supports, under the action of a concentrated moment.

7.4. Example 4: a quarter-thin circular arch with hinged supports. Figure 7.6 Shows the details of a half-circular arch with hinged supports, subjected to a concentrated moment M_o at the middle of the span. This means that at the middle point, the bending moment is expected to be discontinuous. The analytical solutions for central displacement

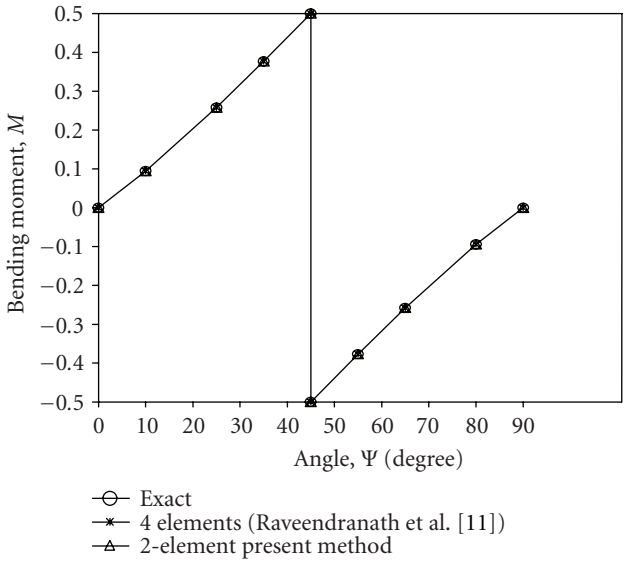

Figure 7.7. Internal bending moment distributions for hinge curved beam.

based on Euler theory of thin beams are reproduced here as follows (Raveendranath et al. [11]):

$$W_c = 0, \tag{7.3a}$$

$$U_c = -0.0100489\frac{M_o \cdot R^2}{EI}, \tag{7.3b}$$

$$\theta_c = 0.1211846\frac{M_o \cdot R}{EI}. \tag{7.3c}$$

In this problem, two elements are used to model this curved beam. Shear effects are neglected in the analysis of this sample problem for the sake of simplicity, as otherwise the explicit calculation of the central deflections calculated via Castigliano's theorem becomes very complicated (Lee and Sin [14]):

$$M = \begin{cases} (1 - \operatorname{Cos}\psi + \operatorname{Sin}\psi)\dfrac{M_o}{2}, & 0 \le \psi \le \dfrac{\pi}{4}, \\ -(1 + \operatorname{Cos}\psi - \operatorname{Sin}\psi)\dfrac{M_o}{2}, & \dfrac{\pi}{4} \le \psi \le \dfrac{\pi}{2}, \end{cases} \tag{7.4a}$$

$$N = -\frac{M_o}{\sqrt{2}R}\operatorname{Sin}\left(\psi - \frac{\pi}{4}\right), \tag{7.4b}$$

$$V = \frac{M_o}{\sqrt{2}R}\operatorname{Cos}\left(\psi - \frac{\pi}{4}\right). \tag{7.4c}$$

The finite element results for the components of displacements are in very good agreement with the above analytical ones. Figures 7.7, 7.8, and 7.9 show, respectively, bending moment, membrane force, and shear force distribution along the arc length calculated at

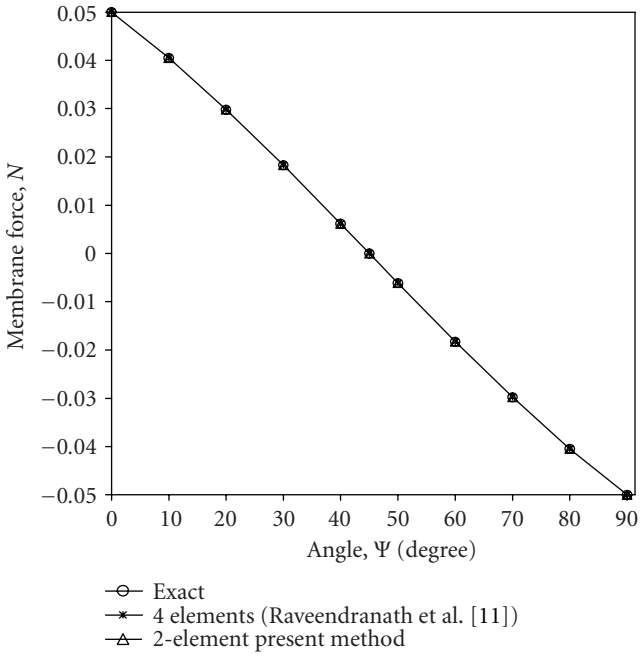

Figure 7.8. Internal memberane force distributions for hinge curved beam.

the nodes and element centered for four elements of the arch using other method. The solutions for two elements model are in very good agreement with the exact solution given by Castigliano's theorem over the entire arc length.

8. Conclusions

A new finite element formulation of the circular arch element was presented in this paper using *Trigonometric function*. Despite other conventional methods which use displacement functions, the element curvature in current study is defined by three nodal curvatures. First the curvature field is defined by trigonometric function while the fundamental relations are derived in polar coordinate for the typical circular arch element. Second, the curvature field in the circular arch is related properly to the three nodal curvatures. This entails that the shape functions are of trigonometric ones. Integration over the curvature enables calculation of the tangential and the radial displacements as well as the sectional rotation between the nodal curvature and displacement is derived by eliminating the rigid displacement components at a typical element node and by using a transformation matrix. Third, minimization of potential energy equation based on internal forces results in force-deformation relation. Last, an algorithm for finite element analysis was presented followed by numerical investigations on typical examples (problems) on curved beams. Four examples were studied in order to verify the validity of the present concept. The results obtained on these typical problems showed that the accuracy of the concept presented is more than those of the other methods. Using the trigonometric functions, the

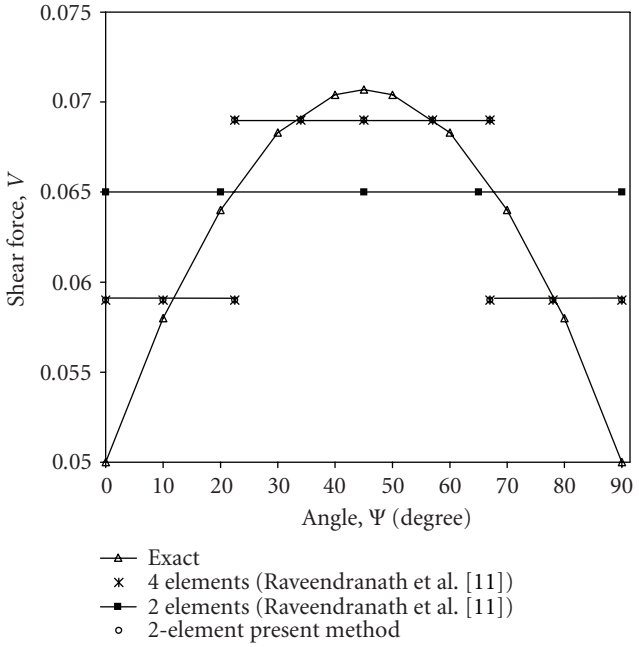

Figure 7.9. Internal shear force distributions for hinge curved beam.

element formulation is largely developed such that only one element can be used to model a curved beam while exact results can be reached. This is because the trigonometric function defines, from the geometrical point of view, the element curvature more accurately. Moreover, since the total potential energy due to axial, shear and bending forces have all been considered in the new formulation, the membrane and shear-locking phenomena have been eliminated. These result in more accurate results compared to those of the other methods.

Symbols

W: Radial displacement
U: Tangential displacement
M_b: Bending moment
V: Shearing force
N: Axial force
κ: Nodal curvature
P_e: Equivalent nodal load vector
R: Radius of arc
A: Cross-section
I: Moment of inertia
E: Young's modulus
G: Shear modulus
χ: Curvature of element
θ: Sectional rotation
γ: Shearing strain
ε: Tangential strain
k: Shear coefficient
δ: Nodal displacement

Appendices

A. Appendix

$$f_1^{\theta} = -\frac{1}{4}\left\{R\,\mathrm{Csc}\left(\frac{L}{4R}\right)^2 \mathrm{Sec}\left(\frac{L}{4R}\right)\mathrm{Sin}\left(\frac{3L}{4R}\right) + \mathrm{Csc}\left(\frac{L}{4R}\right)^2 \mathrm{Sec}\left(\frac{L}{4R}\right)\left(S\,\mathrm{Cos}\left(\frac{L}{4R}\right) + R\,\mathrm{Sin}\left(\frac{3L}{4R}\right) - \frac{S}{R}\right)\right\},$$

$$f_2^{\theta} = -\frac{1}{4}\left\{R\,\mathrm{Csc}\left(\frac{L}{4R}\right)\mathrm{Sec}\left(\frac{L}{4R}\right) + \mathrm{Csc}\left(\frac{L}{4R}\right)^2 \mathrm{Sec}\left(\frac{L}{4R}\right)\left(S\,\mathrm{Cos}\left(\frac{L}{4R}\right) + R\,\mathrm{Sin}\left(\frac{L}{4R}\right) - \frac{S}{R}\right)\right\},$$

$$f_3^{\theta} = \frac{1}{2}\left\{R\,\mathrm{Csc}\left(\frac{L}{4R}\right)^2 \mathrm{Sin}\left(\frac{L}{2R}\right) - \mathrm{Csc}\left(\frac{L}{4R}\right)^2 \left(S\,\mathrm{Cos}\left(\frac{L}{2R}\right) + R\,\mathrm{Sin}\left(\frac{L}{2R}\right) - \frac{S}{R}\right)\right\},$$

$$f_1^{W} = \frac{1}{16R^3}\left\{\left(\mathrm{Csc}\left(\frac{L}{4R}\right)^2 \mathrm{Sec}\left(\frac{L}{4R}\right)\right)\left(4R^5\,\mathrm{Cos}\left(\frac{L}{4R}\right) - \beta R\,\mathrm{Cos}\left(\frac{3L-4S}{4R}\right) - \alpha R^3\,\mathrm{Cos}\left(\frac{3L-4S}{4R}\right)\right) - \left(R^5\,\mathrm{Cos}\left(\frac{3L-4S}{4R}\right) + 2\beta S\,\mathrm{Sin}\left(\frac{3L-4S}{4R}\right) + 2\alpha SR^2\,\mathrm{Sin}\left(\frac{3L-4S}{4R}\right) + 2SR^4\,\mathrm{Sin}\left(\frac{3L-4S}{4R}\right)\right)\right\},$$

$$f_2^{W} = \frac{1}{16R^3}\left\{\left(\mathrm{Csc}\left(\frac{L}{4R}\right)^2 \mathrm{Sec}\left(\frac{L}{4R}\right)\right)\left(4R^5\,\mathrm{Cos}\left(\frac{L}{4R}\right) - \beta R\,\mathrm{Cos}\left(\frac{L-4S}{4R}\right) - \alpha R^3\,\mathrm{Cos}\left(\frac{L-4S}{4R}\right)\right) - \left(R^5\,\mathrm{Cos}\left(\frac{L-4S}{4R}\right) + 2\beta S\,\mathrm{Sin}\left(\frac{L-4S}{4R}\right) + 2\alpha SR^2\,\mathrm{Sin}\left(\frac{L-4S}{4R}\right) + 2SR^4\,\mathrm{Sin}\left(\frac{L-4S}{4R}\right)\right)\right\},$$

$$f_3^{W} = \frac{1}{8R^3}\left\{\left(\mathrm{Csc}\left(\frac{L}{4R}\right)^2\right)\left(-4R^5\,\mathrm{Cos}\left(\frac{L}{2R}\right) + \beta R\,\mathrm{Cos}\left(\frac{L-2S}{2R}\right) + \alpha R^3\,\mathrm{Cos}\left(\frac{L-2S}{2R}\right)\right) + \left(R^5\,\mathrm{Cos}\left(\frac{L-2S}{2R}\right) - 2\beta S\,\mathrm{Sin}\left(\frac{L-2S}{2R}\right) - 2\alpha SR^2\,\mathrm{Sin}\left(\frac{L-2S}{2R}\right) - 2SR^4\,\mathrm{Sin}\left(\frac{L-2S}{2R}\right)\right)\right\},$$

$$f_1^U = \frac{1}{16R^2}\left\{\left(\mathrm{Csc}\left(\frac{L}{4R}\right)^2 \mathrm{Sec}\left(\frac{L}{4R}\right)\right)\left(-4R^5\,\mathrm{Cos}\left(\frac{L}{4R}\right)+4R^3\,\mathrm{Cos}\left(\frac{L}{4R}\right)\right.\right.$$
$$\left.+\beta R\,\mathrm{Cos}\left(\frac{3L-4S}{4R}\right)+\alpha R^3\,\mathrm{Cos}\left(\frac{3L-4S}{4R}\right)\right)$$
$$+\left(R^5\,\mathrm{Cos}\left(\frac{3L-4S}{4R}\right)-4R^4\,\mathrm{Sin}\left(\frac{3L}{4R}\right)\right.$$
$$+4\alpha R^2\,\mathrm{Sin}\left(\frac{3L-4S}{4R}\right)+4R^4\,\mathrm{Sin}\left(\frac{3L-4S}{4R}\right)-2S\beta\,\mathrm{Sin}\left(\frac{3L-4S}{4R}\right)$$
$$\left.\left.-2\alpha SR^2\,\mathrm{Sin}\left(\frac{3L-4S}{4R}\right)-2SR^4\,\mathrm{Sin}\left(\frac{3L-4S}{4R}\right)\right)\right\},$$

$$f_2^U = \frac{1}{16R^2}\left\{\left(\mathrm{Csc}\left(\frac{L}{4R}\right)^2 \mathrm{Sec}\left(\frac{L}{4R}\right)\right)\left(-4R^5\,\mathrm{Cos}\left(\frac{L}{4R}\right)+4R^3\,\mathrm{Cos}\left(\frac{L}{4R}\right)\right.\right.$$
$$\left.+\beta R\,\mathrm{Cos}\left(\frac{L-4S}{4R}\right)+\alpha R^3\,\mathrm{Cos}\left(\frac{L-4S}{4R}\right)\right)$$
$$+\left(R^5\,\mathrm{Cos}\left(\frac{L-4S}{4R}\right)-4R^4\,\mathrm{Sin}\left(\frac{L}{4R}\right)\right.$$
$$+4\alpha R^2\,\mathrm{Sin}\left(\frac{L-4S}{4R}\right)+4R^4\,\mathrm{Sin}\left(\frac{L-4S}{4R}\right)-2S\beta\,\mathrm{Sin}\left(\frac{L-4S}{4R}\right)$$
$$\left.\left.-2\alpha SR^2\,\mathrm{Sin}\left(\frac{L-4S}{4R}\right)-2SR^4\,\mathrm{Sin}\left(\frac{L-4S}{4R}\right)\right)\right\},$$

$$f_3^U = \frac{1}{8R^2}\left\{\left(\mathrm{Csc}\left(\frac{L}{4R}\right)^2\right)\left(4R^5\,\mathrm{Cos}\left(\frac{L}{2R}\right)-4SR^3\,\mathrm{Cos}\left(\frac{L}{2R}\right)\right.\right.$$
$$\left.-\beta R\,\mathrm{Cos}\left(\frac{L-2S}{2R}\right)-\alpha R^3\,\mathrm{Cos}\left(\frac{L-2S}{2R}\right)\right)$$
$$-\left(R^5\,\mathrm{Cos}\left(\frac{L-2S}{2R}\right)+4R^4\,\mathrm{Sin}\left(\frac{L}{2R}\right)-4\alpha R^2\,\mathrm{Sin}\left(\frac{L-2S}{2R}\right)\right.$$
$$-4R^4\,\mathrm{Sin}\left(\frac{L-2S}{2R}\right)+2S\beta\,\mathrm{Sin}\left(\frac{L-2S}{2R}\right)$$
$$\left.\left.+2\alpha SR^2\,\mathrm{Sin}\left(\frac{L-2S}{2R}\right)+2SR^4\,\mathrm{Sin}\left(\frac{L-2S}{2R}\right)\right)\right\},\tag{A.1}$$

where

$$\beta = \frac{IR^2}{A} \qquad \alpha = \frac{EI}{GAk}.\tag{A.2}$$

B. Appendix

$$
\begin{aligned}
V_\theta &= f_\theta \cdot T + f_{\theta 0},\\
V_W &= \left(f_W - f_W\,|_0 \operatorname{Cos}\frac{S}{R} + f_U\,|_0 \operatorname{Sin}\frac{S}{R}\right)\cdot T + f_{W0},\\
V_U &= \left(f_U - f_W\,|_0 \operatorname{Sin}\frac{S}{R} + f_U\,|_0 \operatorname{Cos}\frac{S}{R}\right)\cdot T + f_{U0},\\
f_{\theta 0} &= \begin{bmatrix}0 & 0 & 1 & 0 & 0 & 0\end{bmatrix},\\
f_{W0} &= \begin{bmatrix}\operatorname{Cos}\dfrac{S}{R} & -\operatorname{Sin}\dfrac{S}{R} & R\operatorname{Sin}\dfrac{S}{R} & 0 & 0 & 0\end{bmatrix},\\
f_{U0} &= \begin{bmatrix}\operatorname{Sin}\dfrac{S}{R} & \operatorname{Cos}\dfrac{S}{R} & R\left(1-\operatorname{Cos}\dfrac{S}{R}\right) & 0 & 0 & 0\end{bmatrix}.
\end{aligned}
\tag{B.1}
$$

References

[1] O. C. Zienkiewicz, R. L. Taylor, and J. M. Too, "Reduced integration technique in general analysis of plates and shells," *International Journal for Numerical Methods in Engineering*, vol. 3, no. 2, pp. 275–290, 1971.

[2] H. Stolarski and T. Belytschko, "Membrane locking and reduced integration for curved elements," *Journal of Applied Mechanics*, vol. 49, no. 1, pp. 172–176, 1982.

[3] H. Stolarski and T. Belytschko, "Shear and memberane locking in curved C^0 elements," *Computer Methods in Applied Mechanics and Engineering*, vol. 41, no. 3, pp. 279–296, 1983.

[4] E. D. L. Pugh, E. Hinton, and O. C. Zienkiewicz, "A study of quadrilateral plate bending elements with 'reduced' integration," *International Journal for Numerical Methods in Engineering*, vol. 12, no. 7, pp. 1059–1079, 1978.

[5] J.-L. Batoz, K.-J. Bathe, and L.-W. Ho, "A study of three-node triangular plate bending elements," *International Journal for Numerical Methods in Engineering*, vol. 15, no. 12, pp. 1771–1812, 1980.

[6] A. Tessler and L. Spiridigliozzi, "Curved beam elements with penalty relaxation," *International Journal for Numerical Methods in Engineering*, vol. 23, no. 12, pp. 2245–2262, 1986.

[7] B. D. Reddy and M. B. Volpi, "Mixed finite element methods for the circular arch problem," *Computer Methods in Applied Mechanics and Engineering*, vol. 97, no. 1, pp. 125–145, 1992.

[8] D. G. Ashwell, A. B. Sabir, and T. M. Roberts, "Further studies in the application of curved finite elements to circular arches," *International Journal of Mechanical Sciences*, vol. 13, no. 6, pp. 507–517, 1971.

[9] D. J. Dawe, "Numerical studies using circular arch finite elements," *Computers & Structures*, vol. 4, no. 4, pp. 729–740, 1974.

[10] D. G. Ashwell and A. B. Sabir, "Limitations of certain curved finite elements when applied to arches," *International Journal of Mechanical Sciences*, vol. 13, no. 2, pp. 133–139, 1971.

[11] P. Raveendranath, G. Singh, and B. Pradhan, "A two-noded locking-free shear flexible curved beam element," *International Journal for Numerical Methods in Engineering*, vol. 44, no. 2, pp. 265–280, 1999.

[12] K. J. Bathe, *Finite Element Procedures in Engineering Analysis*, Prentice-Hall, Englewood Cliffs, NJ, USA, 1982.

[13] R. H. Mc Neal and R. C. Harder, *A Proposed Standard Set of Problems to Test Finite Element Accuracy*, North-Holland, Amsterdam, The Netherlands, 1985.

[14] P.-G. Lee and H.-C. Sin, "Locking-free curved beam element based on curvature," *International Journal for Numerical Methods in Engineering*, vol. 37, no. 6, pp. 989–1007, 1994.

[15] A. Sinaie, S. H. Mansouri, H. Saffari, and R. Tabatabaei, "A six-noded locking-free curved beam element based on curvature," *Iranian Journal of Science and Technology*, vol. 27, no. B1, pp. 21–36, 2003.
[16] A. H. Sheikh, "New concept to include shear deformation in a curved beam element," *Journal of Structural Engineering*, vol. 128, no. 3, pp. 406–410, 2002.
[17] K. R. Wen and B. Suhendro, "Nonlinear curved-beam element for arch structures," *Journal of Structural Engineering*, vol. 117, no. 11, pp. 3496–3515, 1991.
[18] R. K. Wen and J. Lange, "Curved beam element for arch buckling analysis," *Journal of the Structural Division, Proceedings of the American Society of Civil Engineers*, vol. 107, no. 11, pp. 2053–2069, 1981.
[19] P. R. Calhoun and D. A. DaDeppo, "Nonlinear finite element analysis of clamped arches," *Journal of Structural Engineering*, vol. 109, no. 3, pp. 599–612, 1983.
[20] S. P. Timoshenko and J. M. Gere, *Theory of Elastic Stability*, McGraw-Hill, New York, NY, USA, 1990.
[21] C. R. Babu and G. Prathap, "A linear thick curved beam element," *International Journal for Numerical Methods in Engineering*, vol. 23, no. 7, pp. 1313–1328, 1986.
[22] G. Shi and G. Z. Voyiadjis, "Simple and efficient shear flexible two-node arch/beam and four-node cylindrical shell/plate finite elements," *International Journal for Numerical Methods in Engineering*, vol. 31, no. 4, pp. 759–776, 1991.
[23] G. Prathap, "The curved beam/deep arch/finite ring element revisited," *International Journal for Numerical Methods in Engineering*, vol. 21, no. 3, pp. 389–407, 1985.

H. Saffari: Department of Civil Engineering, Shahid Bahonar University of Kerman, P.O. Box 133, Kerman 76169, Iran
Email address: hsaffari@mail.uk.ac.ir

R. Tabatabaei: Department of Civil Engineering, Islamic Azad University of Kerman, P.O. Box 7635131167, Kerman 76175-6114, Iran
Email address: tabatabaei@iauk.ac.ir